

Tomography of Band Insulators from Quench Dynamics

Philipp Hauke,^{1,2,*} Maciej Lewenstein,^{3,4} and André Eckardt⁵

¹*Institut für Quantenoptik und Quanteninformation, Österreichische Akademie der Wissenschaften, Technikerstraße 21A, A-6020 Innsbruck, Austria*

²*Institut für Theoretische Physik, Universität Innsbruck, Technikerstraße 25, A-6020 Innsbruck, Austria*

³*ICFO-Institut de Ciències Fotòniques, Parc Mediterrani de la Tecnologia, E-08860 Castelldefels, Spain*

⁴*ICREA-Institució Catalana de Recerca i Estudis Avançats, Lluís Companys 23, E-08010 Barcelona, Spain*

⁵*Max-Planck-Institut für Physik komplexer Systeme, Nöthnitzer Straße 38, D-01187 Dresden, Germany*

(Received 3 February 2014; revised manuscript received 6 May 2014; published 23 July 2014)

We propose a simple scheme for tomography of band-insulating states in one- and two-dimensional optical lattices with two sublattice states. In particular, the scheme maps out the Berry curvature in the entire Brillouin zone and extracts topological invariants such as the Chern number. The measurement relies on observing—via time-of-flight imaging—the time evolution of the momentum distribution following a sudden quench in the band structure. We consider two examples of experimental relevance: the Harper model with π flux and the Haldane model on a honeycomb lattice. Moreover, we illustrate the performance of the scheme in the presence of a parabolic trap, noise, and finite measurement resolution.

DOI: [10.1103/PhysRevLett.113.045303](https://doi.org/10.1103/PhysRevLett.113.045303)

PACS numbers: 67.85.-d, 03.65.Vf, 03.75.Lm, 73.43.-f

Band insulators are a fascinating form of quantum matter. Their very existence relies on band structure and quantum statistics and the geometric phase inherent in their wave function gives rise to intriguing physics: Topological quantum numbers, such as the Chern index or the Z_2 invariant, separate them into classes with fundamentally different behavior [1,2], some of which support chiral or helical edge modes [3,4]. Only recently, first evidence of such topological insulators has been found in solid-state materials [5–7] and photonic systems [8]. The recent creation of artificial gauge fields in optical lattices [9–16] makes it seem likely that topological insulators will be realized in the near future also in highly tunable systems of ultracold atoms. However, the experimental characterization of apparently structureless band insulators poses a challenge. So far, there are schemes that are designed to measure specific topological properties of the system. For example, Zak’s phase, i.e., the Berry phase acquired during the adiabatic motion along a path through the Brillouin zone (BZ), was measured recently from Bloch oscillations [12]. Also, the location of Dirac cones was mapped out in a honeycomb lattice using Landau-Zener transitions [17–19]. Other proposed schemes are designed to directly measure either the Chern number (from density profiles [20], wave-packet dynamics [12,21–24], time-of-flight (TOF) imaging [24–26], or unidirectional TOF imaging with single-site resolution [27]), or to probe the presence of chiral edge modes (via transport measurements [28–31], in particular, using quench-based schemes, or Bragg scattering [32–35]). A method allowing for a full tomography of a band insulator has so far only been proposed for a specific experimental realization of a topological insulator based on spin-dependent hexagonal lattices [36].

Here, we propose a simple scheme for the complete tomography of band-insulating states in one-dimensional (1D) and two-dimensional (2D) optical lattices that is not restricted to a specific system. In particular, the scheme allows for mapping out the Berry curvature as a function of quasimomentum and for measuring the Chern number. Our scheme is based on the momentum-resolved monitoring—via TOF imaging—of the dynamics following an abrupt quench in the band structure. In the following, we first introduce the basic protocol underlying our method, and then discuss two relevant applications: the π -flux Harper model [37,38], and the Haldane model [39].

Scheme for the tomography of band insulators.—Consider spin-polarized (i.e., noninteracting) fermions in a 2D optical lattice. In each elementary cell ℓ , the lattice shall have two sublattice states $s = A, B$, located at $\mathbf{r}_{\ell s}$ [see Fig. 1(a), left]. The corresponding tight-binding Hamiltonian is characterized by matrix elements $h_{\ell' s', \ell s}$ that obey the translational symmetry of the lattice. The diagonal terms refer to on-site potentials, $h_{\ell s, \ell s} \equiv v_s$, and the off-diagonal matrix elements describe tunneling between near neighbors. Thanks to the translational symmetry, the Hamiltonian is diagonal with respect to quasimomentum \mathbf{k} . With respect to the basis states $|\mathbf{k}s\rangle \propto \sum_{\ell} e^{-i\mathbf{k}\cdot\mathbf{r}_{\ell s}} |\ell s\rangle$ it is represented by a \mathbf{k} -dependent 2×2 matrix $h_{s' s}(\mathbf{k}) = \sum_{\ell, \ell'} h_{\ell' s', \ell s} e^{-i(\mathbf{r}_{\ell' s'} - \mathbf{r}_{\ell s})\cdot\mathbf{k}}$, which we decompose as $h_{s' s}(\mathbf{k}) \equiv h_0(\mathbf{k})\delta_{s' s} + \mathbf{h}(\mathbf{k}) \cdot \boldsymbol{\sigma}_{s' s}$. Here, $\boldsymbol{\sigma}_{s' s}$ denotes the vector of Pauli matrices in sublattice space. For every quasimomentum \mathbf{k} , the 2D sublattice space defines a Bloch sphere, with the north and south pole given by $|\mathbf{k}A\rangle$ and $|\mathbf{k}B\rangle$, respectively. The two eigenstates $|\mathbf{k}\pm\rangle$ lie at $\pm\hat{\mathbf{h}}(\mathbf{k})$ on this Bloch sphere, where $\hat{\mathbf{h}}(\mathbf{k}) \equiv \mathbf{h}(\mathbf{k})/|\mathbf{h}(\mathbf{k})| \equiv (\sin(\vartheta_k) \cos(\varphi_k), \sin(\vartheta_k) \sin(\varphi_k), \cos(\vartheta_k))$.

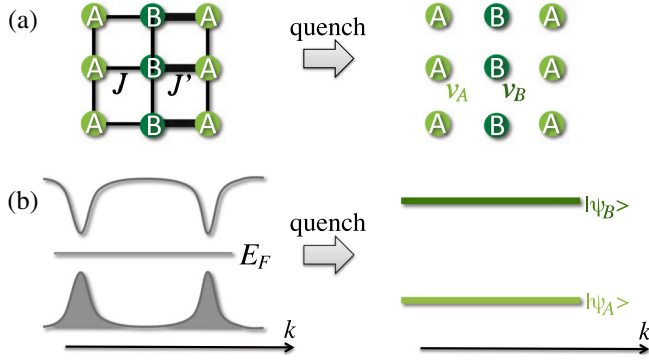


FIG. 1 (color online). General procedure. (a) A lattice with two sublattice states is quenched abruptly such that both sublattices are energetically separated by $\hbar\omega = v_A - v_B$ and tunneling is suppressed (drawn example: a square lattice with alternating tunneling matrix elements J and J'). (b) Initially, the system is a band insulator with the lower band occupied completely. At every quasimomentum \mathbf{k} , the two-dimensional state space is represented by a Bloch sphere, with the state of the lower band lying at $-\hat{\mathbf{h}}(\mathbf{k})$. With the quench, two flat bands are created, onto which the state is projected. The resulting dynamics corresponds to a rotation around the z axis of the Bloch sphere with the same frequency ω for every \mathbf{k} . Monitoring this dynamics in momentum space allows for reconstruction of the initial position on the Bloch sphere, giving a complete tomography of the initial band-insulating state.

Their energies $\varepsilon_{\pm}(\mathbf{k}) = h_0(\mathbf{k}) \pm |\mathbf{h}(\mathbf{k})|$ define the band structure of the lattice.

We consider the system to be in a band-insulating state with complete occupation of the single-particle states of the lower band, $|\mathbf{k}-\rangle = \sin(\vartheta_{\mathbf{k}}/2)|\mathbf{k}A\rangle - \cos(\vartheta_{\mathbf{k}}/2)e^{i\varphi_{\mathbf{k}}}|\mathbf{k}B\rangle$ [40]. Here, we assume that the gap is much larger than the temperature, allowing us to neglect thermal excitations, which would decrease the observed contrast. This band-insulating state is represented by the map $\hat{\mathbf{h}}(\mathbf{k})$ from the first BZ onto the Bloch sphere. The topological properties of this map determine the properties of the system. Our aim is to design a feasible measurement scheme that allows for a reconstruction of $\hat{\mathbf{h}}(\mathbf{k})$.

The momentum (not quasimomentum) distribution of the band insulator, which is obtained from TOF images taken after suddenly switching off the lattice potential, is given by $n(\mathbf{k}) = f(\mathbf{k})|\langle \mathbf{k} - | \mathbf{k}A \rangle + \langle \mathbf{k} - | \mathbf{k}B \rangle|^2 = f(\mathbf{k})[1 - \sin(\vartheta_{\mathbf{k}})\cos(\varphi_{\mathbf{k}})]$. Here, $f(\mathbf{k})$ is a broad envelope function given by the momentum distribution of the Wannier function; the expression in square brackets possesses the periodicity of the reciprocal lattice. Unfortunately, $n(\mathbf{k})$ does not provide sufficient information to reconstruct $\hat{\mathbf{h}}(\mathbf{k})$ or, equivalently, both $\vartheta_{\mathbf{k}}$ and $\varphi_{\mathbf{k}}$. In order to obtain the missing information, at the measurement time t_m the system shall be subjected to an abrupt quench $h_{\ell'\ell_s} \rightarrow h'_{\ell'\ell_s}$, such that a potential offset $v'_A - v'_B \equiv \hbar\omega$ between the A and B sites is created and tunneling suppressed [see Fig. 1(a), right]. In quasimomentum

representation, the Hamiltonian is now characterized by a constant vector $\mathbf{h}'(\mathbf{k}) \approx (\hbar\omega/2)\mathbf{e}_z$ generating a rotation around the z axis of the Bloch sphere with frequency ω . Starting from the band-insulating state, this dynamics is, thus, captured simply by replacing $\varphi_{\mathbf{k}} \rightarrow \varphi_{\mathbf{k}} + \omega(t - t_m)$. This leads to an observable dynamics in the momentum distribution

$$n(\mathbf{k}, t) = f(\mathbf{k})\{1 - \sin(\vartheta_{\mathbf{k}})\cos[\varphi_{\mathbf{k}} + \omega(t - t_m)]\}, \quad (1)$$

whose oscillatory time dependence directly reveals both $\varphi_{\mathbf{k}}$ and $\sin(\vartheta_{\mathbf{k}}) = 1 - |\hat{h}_z(\mathbf{k})|^2$. The time dependence of $n(\mathbf{k}, t)$ allows us to reconstruct $\hat{h}_x(\mathbf{k})$, $\hat{h}_y(\mathbf{k})$, as well as $|\hat{h}_z(\mathbf{k})|$ from the amplitude and the phase of the oscillations. It is sufficient to consider data for \mathbf{k} from the first BZ; the Wannier envelope $f(\mathbf{k})$ does not spoil the measurement as it just gives an irrelevant overall prefactor for each value of \mathbf{k} . For a full tomography, it remains to reveal the sign of $\hat{h}_z(\mathbf{k})$. Since the overall sign is not important, one has to determine those lines where $\hat{h}_z(\mathbf{k})$ changes sign. These lines can be clearly identified by a characteristic cusplike behavior of $|\hat{h}_z(\mathbf{k})|$, $|\hat{h}_z(\mathbf{k})| \propto |\mathbf{k} - \mathbf{k}_{\text{sign change}}|$, which sharply contrasts with the smooth variation of $\hat{h}_z(\mathbf{k})$ as it results from tunneling between near neighbors.

Moreover, $h_z(\mathbf{k})$, including its sign, can also be measured via band mapping: After abruptly switching on a strong potential offset lifting B with respect to A sites as before, the lattice is switched off without waiting time at a slow rate such that quasimomentum is mapped onto momentum. Absorption images after TOF reveal then a momentum distribution where the A (B) population, corresponding to the lowest (first excited) band, is mapped onto the first (second) BZ.

Edge states in the Harper model with π flux.— Once $\hat{\mathbf{h}}(\mathbf{k})$ is reconstructed, one can infer whether the system supports edge modes or not, by invoking the bulk-boundary correspondence. According to the procedure derived in Ref. [41], for that purpose one has to identify a closed path $\mathbf{k}(\lambda)$ in \mathbf{k} space such that $\hat{\mathbf{h}}(\mathbf{k}(\lambda))$ lies in a plane \mathcal{E} that contains the origin (i.e., it lies on a great circle of the Bloch sphere). If the unit vector $\hat{\mathbf{h}}$ describes a closed circle around the origin when moving along the path, the system does possess zero-energy edge modes; if not, it does not.

Motivated by recent experiments [15,16], let us consider the example of a square lattice with nearest-neighbor tunneling and with a flux of π (half a flux quantum) per plaquette, which can be generated via laser-assisted tunneling or lattice shaking [42]. We consider a gauge where the tunneling matrix elements in the y direction alternate between $-J$ and $+J$ when moving through the lattice in the x direction, giving two inequivalent sublattices $s = A, B$. Additionally, we assume different on-site energies $v_A = \Delta/2$ and $v_B = -\Delta/2$, and that the tunneling matrix element in the x direction alternates between $-J'$ and $-J$ [Fig. 1(a)]; both can be achieved by a superlattice in the x direction.

The extent of the first BZ is given by π (2π) in the k_x (k_y) direction. The quasimomentum-space Hamiltonian of this model is characterized by

$$\mathbf{h}(\mathbf{k}) = (-J - J' \cos(2k_x), J' \sin(2k_x), -2J \cos(k_y) + \Delta). \quad (2)$$

The two parameters Δ/J and J'/J allow us to explore various situations with qualitatively different band structures. Most notably, for $J = J'$ and $\Delta < 2J$, one finds two Dirac cones lying at $k_x = \pm\pi/2$ and $k_y = \arccos(\Delta/2J)$. For imbalanced tunneling matrix elements $J' \neq J$, a band gap opens at the Dirac points and edge states appear if $J' > J$. We focus here on the case $\Delta = 0$ (for $\Delta \neq 0$ see [43]). In this case, by choosing $k_y^0 = \pi/2$ ($\hat{h}_z = 0$), we can confine $\hat{\mathbf{h}}_{k_y^0}(k_x)$ to a plane that contains the origin of $\hat{\mathbf{h}}$'s Bloch sphere, a necessary condition for observing edge modes at zero energy [41]. Edge states (in the equivalent system with open boundary conditions in the x direction) do appear if the origin is encircled by $\hat{\mathbf{h}}_{k_y^0}(k_x)$ [41].

In an experiment, we wish to reconstruct $\hat{\mathbf{h}}_{k_y^0}(k_x)$ from the dynamics following a sublattice quench in order to conclude whether the system possesses edge states or not. A typical result will look like the upper row of Fig. 2, where we plot $n(\mathbf{k}, t)$ at $k_y^0 = \pi/2$, $\Delta = 0$, and four values of J'/J . In order to illustrate the robustness of our method, we have contaminated $n(\mathbf{k}, t)$ with normal-distributed uncorrelated noise, with a standard deviation of 10% of the average signal. Furthermore, we assumed a mediocre experimental resolution of 21 points in the first BZ along k_x and 41 points in time. We can reconstruct $\hat{\mathbf{h}}_{k_y^0}(k_x)$ from $n(k_x, k_y^0; t)$ simply by identifying $\varphi(\mathbf{k})$ with the position of the first maximum

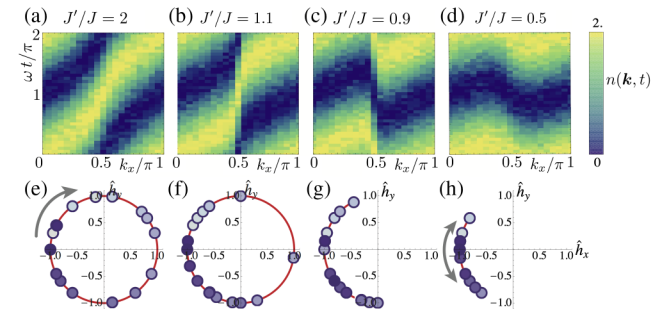


FIG. 2 (color online). (a)–(d) Time-resolved TOF images for the π -flux Harper model ($\Delta = 0$ and $k_y^0 = \pi/2$). To mimic a realistic experiment, we added normal-distributed noise with a standard deviation of 0.1 of the average signal and assumed a limited resolution of 21 points along k_x and 41 time points. (e)–(f) If edge states are supported, the temporal maximum as a function of quasimomentum winds around the time period once [panels (a),(b)], and $\hat{\mathbf{h}}_{k_y^0}(k_x) = (\hat{h}_x, \hat{h}_y, 0)$ describes a unit circle around the origin (e),(f), contrary to when no edge state is supported (c),(d) and (g),(h), respectively). Red line: exact case. Bullets: values extracted from the noisy, resolution-limited data of the upper row, using Eq. (1) [k_x from 0 (light) to π (dark)].

in time and $\sin(\vartheta_k) = 1 - |\hat{h}_z(\mathbf{k})|^2$ with the difference between maximum and minimum. The resulting graphs $\hat{\mathbf{h}}_{k_y^0}(k_x) = (\hat{h}_x, \hat{h}_y, 0)$, plotted in the lower row of Fig. 2, clearly reveal the presence or absence of edge states: Edge states, expected for the two plots on the left where $J' > J$, are clearly indicated by data points describing a circle around the origin. Qualitatively, one can see this information already in the time evolution of $n(k_x, k_y^0; t)$ in the upper row: If the band insulator supports edge states, the maximum winds around the time period.

Our scheme also permits us to monitor the topological transition of the model happening when Δ exceeds $2J$, where for $J' = J$ both Dirac cones merge (see [43], where edge modes for open boundary conditions are discussed also).

Measuring Berry curvature and Chern number in a Haldane-like system.— Edge currents are topologically protected only if the associated integer Chern number, given by the integral of the Berry curvature over the whole BZ, is finite. In the above example, this is not the case, since the edge modes always appear in counterpropagating pairs located at the two Dirac cones. We now turn to a lattice model where a finite Chern number can be found and demonstrate how our scheme can be used to map out the Berry curvature in quasimomentum.

The Berry curvature of the lower band is given by

$$\Omega_-(\mathbf{k}) = \frac{1}{2} (\partial_{k_x} \hat{\mathbf{h}} \times \partial_{k_y} \hat{\mathbf{h}}) \cdot \hat{\mathbf{h}}, \quad (3)$$

and is readily obtained from $\hat{\mathbf{h}}(\mathbf{k})$. It describes the polarizability [44] and the anomalous Hall conductivity [45] also at lower filling. The Chern number reads

$$w_- = \frac{1}{2\pi} \int d^2k \Omega_-(\mathbf{k}). \quad (4)$$

It counts how often $\hat{\mathbf{h}}(\mathbf{k})$ wraps around the Bloch sphere when \mathbf{k} covers the full first BZ. It is proportional to the Hall conductivity of the completely filled band and indicates the presence of robust chiral edge modes [3].

Let us consider the Haldane-like model sketched in Fig. 3(a) with the lower band completely filled. The atoms live on a honeycomb lattice [17,46] with real tunneling matrix elements J between nearest neighbors (NNs) and complex tunneling matrix elements $J'e^{i\theta}$ with Peierls phase θ between next-nearest neighbors (NNNs). The model can be realized, e.g., in a shaken optical lattice [47]. For $J' = 0$, the vector $\mathbf{h}(\mathbf{k})$ lies in the xy plane and the band structure possesses two Dirac points where $\mathbf{h}(\mathbf{k}) = 0$. For finite NNN tunneling, $J' > 0$, $\hat{h}_z(\mathbf{k})$ acquires a finite value and a direct band gap opens at the Dirac cones (though one still has an indirect band touching). While for $J' = 0$ the unit vector $\hat{\mathbf{h}}(\mathbf{k})$ was confined to the equator, when approaching the Dirac points it will now visit either the north or the south pole, depending on the sign of $\hat{h}_z(\mathbf{k})$. The unit vector

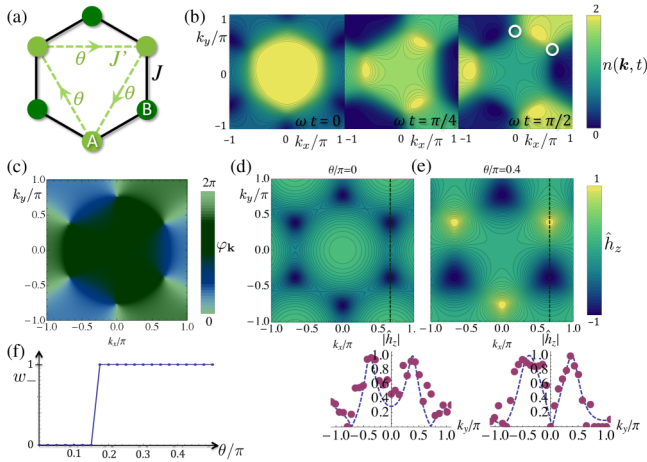


FIG. 3 (color online). (a) Haldane-like lattice model with real tunneling parameter J and complex tunneling parameter $J'e^{i\theta}$. (b) $n(\mathbf{k}, t)$ changes strongly with time ($J' = 0.3J$, $\theta = 0.4\pi$). (c) The winding of the phase $\varphi_{\mathbf{k}}$ is opposite around the two Dirac points [white circles in (b)], independently of θ . (d), (e) In the topologically trivial phase (d, $J' = 0.3J$ and $\theta = 0$), the plotted quantity \hat{h}_z has the same sign at the two Dirac cones, while in the topological phase [(d), $J' = 0.3J$ and $\theta = 0.4\pi$] it has opposite sign; this sign change is clearly visible as a kink in the measured quantity $|\hat{h}_z|$ (lower plots showing $|\hat{h}_z|$ along the dashed lines; lines: ideal case, bullets: data for trapped system with normal-distributed noise of variance 0.05, using realistic parameters [13,15], $J/\hbar = 2\pi \times 0.26$ kHz, $\omega = 2\pi \times 10$ kHz, trapping frequency $2\pi \times 50$ Hz, lattice spacing 380 nm). (f) The coarse-grained Chern number computed following Ref. [48] reproduces the exact result already for a limited resolution of 4×4 reciprocal lattice points.

$\hat{\mathbf{h}}(\mathbf{k})$ can only wrap around the Bloch sphere as required for a finite Chern number if $\hat{h}_z(\mathbf{k})$ has opposite sign at the two Dirac points such that it visits both poles. We find that, while for $|\theta| < \theta_c$ the system is a trivial band insulator, it becomes a topological Chern insulator, characterized by a Chern number $|w_-| = 1$, once $|\theta| > \theta_c \approx 0.18\pi$.

As exemplified in Fig. 3(b) for an initial state in the topological phase ($\theta = \pi/2$), $n(\mathbf{k}, t)$ changes its pattern strongly as a function of time. From this dynamics we can extract the position of $\hat{\mathbf{h}}(\mathbf{k})$ on the Bloch sphere [Figs. 3(c)–3(e)]. The sign change of \hat{h}_z for $\theta/\pi > 0.18$ [Fig. 3(e)] between the two Dirac cones identifies a finite Chern number $|w_-| = 1$. Although within our scheme one can directly measure only the absolute value $|\hat{h}_z|$, the sign change in $\hat{h}_z(\mathbf{k})$ can clearly be identified from the pronounced kink where $|\hat{h}_z|$ touches zero, either between the two Dirac cones, indicating the topological phase [Fig. 3(e)], or elsewhere, as in the trivial phase [Fig. 3(d)]. The fact that the sign change of $h_z(\mathbf{k})$ can occur between the Dirac cones, where the band gap is largest, allows us to indirectly identify a topological band structure even if the system is not in a perfect band-insulating state. Namely, thermal excitations or small deviations from unit filling are

relevant mainly near the Dirac cones, and not where the sign change occurs.

In a realistic situation, the resolution of $n(\mathbf{k}, t)$ will be restricted. Approximating the Chern number (4) by a sum over differences is unreliable close to the topological transition (see [43]). Much better results are obtained by the gauge-invariant description in terms of effective field strengths developed by Fukui, Hatsugai, and Suzuki [48]. In the Supplemental Material [43], we show how their formula can be expressed in terms of $\hat{\mathbf{h}}$. Since this method enforces an integer result, it gives the exact answer already for very small numbers of reciprocal lattice points. We demonstrate this in Fig. 3(f), where we use for $n(\mathbf{k})$ only 4×4 coarse-grained pixels in the first BZ and take only 10 time steps. We again obtain $\sin \theta_{\mathbf{k}}$ from the maximal amplitude of the data points and $\varphi_{\mathbf{k}}$ from the position of the maximum (for such a low resolution, the sign of h_z can be obtained from band mapping). Remarkably, even for this extremely resolution-limited situation, the Chern number can be reproduced accurately.

A natural question concerns the role of the trapping potential. As shown in [43], a harmonic trap modifies the measured momentum distribution (1) roughly by a prefactor $(\mu_0 - \epsilon_-(\mathbf{k})/\mu_0 - \epsilon_{\min})^2 \text{sinc}^2([\mu_0 - \epsilon_-(\mathbf{k})]t/2)$, with Fermi energy μ_0 and band minimum ϵ_{\min} . The first term describes the reduced contrast of modes with high energy, since these are only populated in the central region of the trap, and the second term captures dephasing during the postquench time evolution, caused by the spatially varying potential energy. For realistic parameters, both effects are small, and the proposed scheme works reliably even in the presence of a trap [43] (cf. the lower panels of Fig. 3). A newer generation of experiments may enable avoiding a spatially varying trapping potential altogether [49].

Discussion, conclusion, and outlook.— The robust and simple method for the tomography of band insulators described here is not restricted to the two discussed examples. It can be applied to any 1D or 2D band insulator with two states per elementary lattice cell—interesting examples include the Su-Schrieffer-Heeger [50] or Rice-Mele model [51], which was recently realized in an optical lattice [12]. Here, an interesting application would be to measure a topological charge pump [52] to extract the Chern number quantizing the transport of matter. Moreover, the method can also be employed to measure systems with only a partially filled lowest band, and it provides a means to validate Hamiltonians synthesized for the purpose of quantum simulation. As an outlook, it will be interesting to generalize the scheme to lattices with more than two sublattice states and to include internal atomic states.

We acknowledge discussions with Alexander Szameit and Leticia Tarruell. This work was supported by the EU IP SIQS, EU STREP EQuAM, ERC AdG OSYRIS, ERC synergy Grant UQUAM, Fundació Cellex, and SFB FoQuS (FWF Project No. F4006-N16).

- * philipp.hauke@uibk.ac.at
- [1] A. Kitaev, *Advances In Theoretical Physics: Landau Memorial Conference Chernogolokova (Russia)*, AIP Conf. Proc. No. 1134 (AIP, New York, 2008), p. 22.
- [2] S. Ryu, A. P. Schnyder, A. Furusaki, and A. W. W. Ludwig, *New J. Phys.* **12**, 065010 (2010).
- [3] M. Z. Hasan and C. L. Kane, *Rev. Mod. Phys.* **82**, 3045 (2010).
- [4] X. Qi and S. Zhang, *Rev. Mod. Phys.* **83**, 1057 (2011).
- [5] D. Kim, S. Thomas, T. Grant, J. Botimer, Z. Fisk, and J. Xia, *Sci. Rep.* **3**, 3150 (2013).
- [6] X. Zhang, N. P. Butch, P. Syers, S. Ziemak, R. L. Greene, and J. Paglione, *Phys. Rev. X* **3**, 011011 (2013).
- [7] P. Gehring, H. M. Benia, Y. Weng, R. Dinnebier, C. R. Ast, M. Burghard, and K. Kern, *Nano Lett.* **13**, 1179 (2013).
- [8] M. C. Rechtsman, Y. Plotnik, J. M. Zeuner, D. Song, Z. Chen, A. Szameit, and M. Segev, *Phys. Rev. Lett.* **111**, 103901 (2013).
- [9] M. Aidelsburger, M. Atala, S. Nascimbène, S. Trotzky, Y.-A. Chen, and I. Bloch, *Phys. Rev. Lett.* **107**, 255301 (2011).
- [10] K. Jiménez-García, L. J. LeBlanc, R. A. Williams, M. C. Beeler, A. R. Perry, and I. B. Spielman, *Phys. Rev. Lett.* **108**, 225303 (2012).
- [11] J. Struck, C. Ölschläger, M. Weinberg, P. Hauke, J. Simonet, A. Eckardt, M. Lewenstein, K. Sengstock, and P. Windpassinger, *Phys. Rev. Lett.* **108**, 225304 (2012).
- [12] M. Atala, M. Aidelsburger, J. T. Barreiro, D. Abanin, T. Kitagawa, E. Demler, and I. Bloch, *Nat. Phys.* **9**, 795 (2013).
- [13] J. Struck, M. Weinberg, C. Ölschläger, P. Windpassinger, J. Simonet, K. Sengstock, R. Höppner, P. Hauke, A. Eckardt, M. Lewenstein, and L. Mathey, *Nat. Phys.* **9**, 738 (2013).
- [14] C. V. Parker, L.-C. Ha, and C. Chin, *Nat. Phys.* **9**, 769 (2013).
- [15] M. Aidelsburger, M. Atala, M. Lohse, J. T. Barreiro, B. Paredes, and I. Bloch, *Phys. Rev. Lett.* **111**, 185301 (2013).
- [16] H. Miyake, G. A. Siviloglou, C. J. Kennedy, W. C. Burton, and W. Ketterle, *Phys. Rev. Lett.* **111**, 185302 (2013).
- [17] L. Tarruell, D. Greif, T. Uehlinger, G. Jotzu, and T. Esslinger, *Nature (London)* **483**, 302 (2012).
- [18] L.-K. Lim, J.-N. Fuchs, and G. Montambaux, *Phys. Rev. Lett.* **112**, 155302 (2014).
- [19] L.-K. Lim, J.-N. Fuchs, and G. Montambaux, *Phys. Rev. Lett.* **108**, 175303 (2012).
- [20] R. O. Umucalilar, H. Zhai, and M. O. Oktel, *Phys. Rev. Lett.* **100**, 070402 (2008).
- [21] H. M. Price and N. R. Cooper, *Phys. Rev. A* **85**, 033620 (2012).
- [22] D. A. Abanin, T. Kitagawa, I. Bloch, and E. Demler, *Phys. Rev. Lett.* **110**, 165304 (2013).
- [23] A. Dauphin and N. Goldman, *Phys. Rev. Lett.* **111**, 135302 (2013).
- [24] X.-J. Liu, K. T. Law, T. K. Ng, and P. A. Lee, *Phys. Rev. Lett.* **111**, 120402 (2013).
- [25] M. Burrello, I. C. Fulga, E. Alba, L. Lepori, and A. Trombettoni, *Phys. Rev. A* **88**, 053619 (2013).
- [26] E. Zhao, N. Bray-Ali, C. J. Williams, I. B. Spielman, and I. I. Satija, *Phys. Rev. A* **84**, 063629 (2011).
- [27] L. Wang, A. A. Soluyanov, and M. Troyer, *Phys. Rev. Lett.* **110**, 166802 (2013).
- [28] N. Goldman, I. Satija, P. Nikolic, A. Bermudez, M. A. Martin-Delgado, M. Lewenstein, and I. B. Spielman, *Phys. Rev. Lett.* **105**, 255302 (2010).
- [29] N. Goldman, J. Dalibard, A. Dauphin, F. Gerbier, M. Lewenstein, P. Zoller, and I. B. Spielman, *Proc. Natl. Acad. Sci. U.S.A.* **110**, 6736 (2013).
- [30] M. Killi and A. Paramekanti, *Phys. Rev. A* **85**, 061606(R) (2012).
- [31] M. Killi, S. Trotzky, and A. Paramekanti, *Phys. Rev. A* **86**, 063632 (2012).
- [32] X.-J. Liu, X. Liu, C. Wu, and J. Sinova, *Phys. Rev. A* **81**, 033622 (2010).
- [33] T. D. Stanescu, V. Galitski, and S. Das Sarma, *Phys. Rev. A* **82**, 013608 (2010).
- [34] M. Buchhold, D. Cocks, and W. Hofstetter, *Phys. Rev. A* **85**, 063614 (2012).
- [35] N. Goldman, J. Beugnon, and F. Gerbier, *Phys. Rev. Lett.* **108**, 255303 (2012).
- [36] E. Alba, X. Fernandez-Gonzalvo, J. Mur-Petit, J. K. Pachos, and J. J. García-Ripoll, *Phys. Rev. Lett.* **107**, 235301 (2011).
- [37] P. Harper, *Proc. Phys. Soc. London Sect. A* **68**, 874 (1955).
- [38] D. Hofstadter, *Phys. Rev. B* **14**, 2239 (1976).
- [39] F. D. M. Haldane, *Phys. Rev. Lett.* **61**, 2015 (1988).
- [40] Our measurement scheme itself is robust also when approaching the limit of an enhanced translational symmetry where both sublattice states become equivalent. However, in this trivial limit the band gap closes, impeding the preparation of the band insulator.
- [41] S. Ryu and Y. Hatsugai, *Phys. Rev. Lett.* **89**, 077002 (2002).
- [42] N. Goldman, G. Juzeliunas, P. Ohberg, and I. B. Spielman, arXiv:1308.6533 [Rep. Prog. Phys. (to be published)].
- [43] See Supplemental Material at <http://link.aps.org/supplemental/10.1103/PhysRevLett.113.045303> for useful details for observing topological phase transitions in the Harper and Haldane models, and for a discussion of the influence of a trapping potential.
- [44] D. Xiao, M.-C. Chang, and Q. Niu, *Rev. Mod. Phys.* **82**, 1959 (2010).
- [45] F. D. M. Haldane, *Phys. Rev. Lett.* **93**, 206602 (2004).
- [46] P. Soltan-Panahi, J. Struck, P. Hauke, A. Bick, W. Plenkers, G. Meineke, C. Becker, P. Windpassinger, M. Lewenstein, and K. Sengstock, *Nat. Phys.* **7**, 434 (2011).
- [47] P. Hauke, O. Tieleman, A. Celi, C. Ölschläger, J. Simonet, J. Struck, M. Weinberg, P. Windpassinger, K. Sengstock, M. Lewenstein, and A. Eckardt, *Phys. Rev. Lett.* **109**, 145301 (2012).
- [48] T. Fukui, Y. Hatsugai, and H. Suzuki, *J. Phys. Soc. Jpn.* **74**, 1674 (2005).
- [49] A. L. Gaunt, T. F. Schmidutz, I. Gotlibovych, R. P. Smith, and Z. Hadzibabic, *Phys. Rev. Lett.* **110**, 200406 (2013).
- [50] W. P. Su, J. R. Schrieffer, and A. J. Heeger, *Phys. Rev. Lett.* **42**, 1698 (1979).
- [51] M. J. Rice and E. J. Mele, *Phys. Rev. Lett.* **49**, 1455 (1982).
- [52] L. Wang, M. Troyer, and X. Dai, *Phys. Rev. Lett.* **111**, 026802 (2013).